Research Article

Adnan*, Umar Khan, Naveed Ahmed, D. Baba Basha, Syed Tauseef Mohyud-Din, Omar Mahmoud, and Ilyas Khan*

Numerical investigation of heat transfer in the nanofluids under the impact of length and radius of carbon nanotubes

https://doi.org/10.1515/phys-2022-0040
received March 25, 2021; accepted May 05, 2022

Abstract: The investigation of thermal transport in the nanofluid over a curved Riga surface is significant and extensively used in many industries as well as in engineering. Therefore, the study is conducted to analyze the thermal transport rate in H_2O composed of nanomaterial, namely, carbon nanotubes (CNTs). To improve the thermal conductance, a thermal conductivity correlation based on the length and radius of CNTs is plugged in the energy equation. After that, the flow model was reduced into a self-similar form *via* feasible transformations and tackled numerically. From the plotted results, it is experienced that the nanofluid velocity drops against a more curved surface. The momentum boundary layer intensifies against larger curvature. An enhanced temperature is experienced in the nanofluid due to varying the parameters. Further, thermal conductivity of the nanofluids rises due to the high volume fraction factor, which plays a significant role in thermal transport. Moreover, the local thermal performance rises linearly against M.

Keywords: curved Riga surface, carbon nanotubes, curvature, Yamada and Ota model, heat transfer, numerical scheme

*** Corresponding author: Adnan,** Department of Mathematics, Mohi-ud-Din Islamic University, Nerian Sharif, AJ&K 12080, Pakistan, e-mail: adnan_abbasi89@yahoo.com
*** Corresponding author: Ilyas Khan,** Department of Mathematics, College of Science Al-Zulfi, Majmaah University, Al-Majmaah 11952, Saudi Arabia, e-mail: i.said@mu.edu.sa
Umar Khan: Department of Mathematics and Statistics, Hazara University, Mansehra 21120, Pakistan
Naveed Ahmed: Department of Mathematics, Faculty of Sciences, HITEC University, Taxila Cantt 47070, Pakistan
D. Baba Basha: Department of Physics, College of Computer and Information Sciences Majmaah University, Al-Majmaah, 11952, Saudi Arabia
Syed Tauseef Mohyud-Din: Department of Mathematics, University of Multan, Multan 66000, Pakistan
Omar Mahmoud: Petroleum Engineering Department, Faculty of Engineering and Technology, Future University in Egypt, New Cairo 11845, Egypt

Nomenclature

$U^\star$, $V^\star$	the velocities in s and r directions, respectively
$p^\star$	pressure
$\breve{\rho}_{nf}$	density of the nanofluids
$\breve{k}_{nf}$	thermal conductivity
$(\overline{\rho \breve{C}_p})_{nf}$	heat capacity
$T^\star$	temperature
nf	stands for nanofluid
ϕ	volume fraction
$\breve{\rho}_f$	H_2O density
$\breve{\rho}_{cnt}$	CNTs density
$(\overline{\rho \breve{C}_p})_f$	H_2O heat capacity
$(\overline{\rho \breve{C}_p})_{cnt}$	CNTs heat capacity
L	length of CNTs
R	radius of CNTs
$\breve{k}_f$	thermal conductivity of H_2O
$\breve{k}_{cnt}$	thermal conductivity of CNTs
$\breve{\mu}_{nf}$	dynamic viscosity
$\breve{\mu}_f$	dynamic viscosity of H_2O
C_F	skin friction
Nu	Nusselt number
q_w	heat flux
τ_{rs}	shear stress
η	similarity variable
$F(\eta)$	dimensionless velocity
$\beta(\eta)$	dimensionless temperature
Θ	modified Hartmann number
M	thermal slip number
λ^*	reciprocal magnetic Prandtl number
γ	partial slip number

K_1^*	micropolar parameter
n	microgyration parameter
λ_1^*	slip parameter
ω^*	non-dimensional parameter

1 Introduction

Heat transfer analysis by considering the impacts of various physical phenomena like an imposed magnetic field, thermal radiation, and resistive heating is of great significance and a fascinating topic for more researchers, engineers, and industrialists. For many industrial and engineering purposes, a huge amount of heat transfer is required which accomplishes the process of many industrial products. Unlikely, the regular liquids failed to provide the required heat transfer characteristics. To reduce these issues faced by the engineers, industrialists, and scientists, a new effective class of fluids was required which successfully overcame the aforementioned problems. Therefore, a class of fluids was developed by dispersing the nanoscaled particles of various metal oxides, metals, carbon nanotubes (CNTs) and ferromagnetic in the regular liquid's kerosene oil, ethylene glycol (EG), *etc*. This newly developed fluid became very popular due to its vital thermal performance. The new class of fluids is named as "nanofluids" in which the nanomaterial and host fluid is thermally compatible with a large amount of heat transfer properties. The nanofluids strengthen its roots in medical sciences, biotechnology, electronics, computer chips, electrical engineering, and in the manufacturing of home appliances.

Thermal conductivity of the nanoparticles and host liquids significantly interfere in the heat transfer analysis of resultant fluid namely nanofluid. Therefore, several thermal conductivity models were proposed by incorporating various factors like different shapes of nanomaterial, length and radius of CNTs, *etc*. A thermal conductance correlation particularly for spherical type nanoparticles was reported in ref. [1]. The nanoparticles shape factor-based model was developed by Hamilton [2]. The particular deals with blades, bricks, platelets and cylindrical shaped nanoparticles. A reliable thermal conductance correlation for EG and oil suspended by copper oxide was proposed by Koo and Kleinstreuer [3,4]. They incorporated the temperature factor in the correlation for better heat transfer phenomena. The extended version of Hamilton model was reported in ref. [5] by taking the shape factor equal to three.

A reliable thermal conductivity correlation for the mixture of water and aluminum oxide Al_2O_3 nanoparticles was developed by Li and Peterson [6]. For better heat transfer performance of the correlation, they used fraction and temperature factors in the model and found an excellent performance of the model. For metallic and oxides nanoparticles supported thermal conductivity correlation developed by Patel *et al.* [7]. They introduced the effects of particles and temperature to enhance the performance of the model. In 2010, Godson *et al.* [8] proposed a thermal conductivity model for gold/water nanofluid and explored interesting results. Thermal conductivity model for Al_2O_3/H_2O nanofluid was reported by Corcione [9]. The model comprised the influences of freezing temperature and found the results for the proposed model.

The proposed thermal conductivity models attained much interest of the researchers, engineers, and scientists and they focused on the heat transfer investigation in the nanofluids by incorporating the various thermal conductance correlations in the energy equation. The heat transfer investigation in the nanofluid by implementing the KKL thermal conductivity correlation was reported by Sheikholeslami *et al.* [10].

Another nanomaterial termed as CNTs has remarkable mechanical and heat transfer characteristics due to high thermal conductivity. Thus, due to exciting heat transfer rate, CNTs have become very famous among the researchers. Therefore, heat transfer investigation by implementing CNTs-based thermal conductivity in the nanofluid models was reported and the contribution of CNTs in the heat transfer phenomena was found fascinating. In 2005, Xu [11] proposed thermal conductivity model for CNTs. In 2017, Saleh *et al.* [12] examined the heat transfer analysis in micropolar fluid of unsteady nature over a curved surface. The surface is permeable and capable of stretching and shrinking. They examined the significant role of CNTs-based thermal conductivity of the nanofluid in the heat transfer characteristics. In 2018, Ahmad and Khan [13] modeled the flow of Sisko nanofluid over a curved surface moving in cylindrical coordinates.

Reddy *et al.* [14] discussed the dual solutions for nanofluid model over curved geometry. The effects of nonlinear thermal radiations and cross diffusion gradients are embedded in the energy and concentration equations. Saba *et al.* [15] examined the flow of nanofluid over curved surface and examined the results for nanofluid velocity.

From literature study, it is revealed that the flow of nanofluid by implementing two different thermal conductivity models and the influence of length and radius of CNTs over curved Riga surface are not presented so far. Therefore, this study is carried out to fill this research gap. Two different nanofluid models are discussed on the bases of two thermal conductivity models. Numerical treatment is adopted for the solution and graphical results.

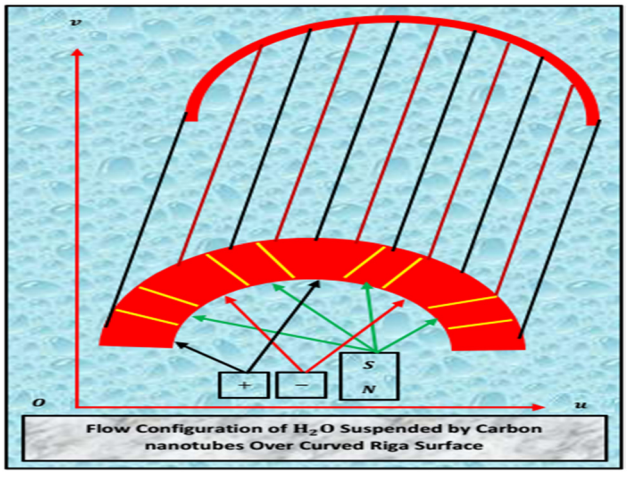

Figure 1: Flow of H_2O suspended by CNTs over curved Riga surface.

2 Mathematical modeling of the model

2.1 Problem statement and geometry

The flow of water suspended by CNTs is considered over a curved Riga surface. The Riga surface is situated in the curvilinear coordinate system. The curve radius is denoted by R, wherears r and S are curvilinear coordinates. It is presumed that the colloidal suspension is thermally compatible. Moreover, the fluid is viscous and incompressible. Figure 1 highlights the flow configuration of water saturated by CNTs.

2.2 Governing model

By using the abovementioned assumptions, the following are the governing equations for the particular nanofluid flow over a curved Riga surface [16]:

$$\frac{\partial}{\partial r}(V^{\star}(r+R^{\star}))+R^{\star}\frac{\partial U^{\star}}{\partial S}=0, \tag{1}$$

$$\frac{\partial}{\partial r}(H_1^{\star}(r+R^{\star}))+R^{\star}\frac{\partial H_2^{\star}}{\partial S}=0, \tag{2}$$

$$\frac{U^{\star 2}}{r+R^{\star}}-\frac{1}{\breve{\rho}_{nf}}\frac{\partial p^{\star}}{\partial r}=0, \tag{3}$$

$$\begin{aligned}&\left(V^{\star}\frac{\partial U^{\star}}{\partial r}+\frac{R^{\star}U^{\star}}{r+R^{\star}}\frac{\partial U^{\star}}{\partial S}+\frac{V^{\star}U^{\star}}{r+R^{\star}}\right)+\frac{1}{\breve{\rho}_{nf}}\left(\frac{1}{r+R^{\star}}\right)\frac{\partial p^{\star}}{\partial s}\\&=\left(\frac{\breve{\mu}_{nf}}{\breve{\rho}_{nf}}+\frac{K^{\star}}{\rho_{nf}^{\star}}\right)\left(\frac{\partial^2 U^{\star}}{\partial r^2}-\frac{U^{\star}}{(r+R^{\star})^2}+\frac{1}{r+R^{\star}}\frac{\partial U^{\star}}{\partial r}\right)\\&\quad-\frac{K^{\star}}{\breve{\rho}_{nf}}\frac{\partial N^{\star}}{\partial r}+\frac{\pi J_0^{\star}M_0^{\star}}{8\breve{\rho}_{nf}}e^{-\frac{\pi}{a}r}+\frac{\mu_e^{\star}}{4\pi\rho_e}\left(\left(\frac{R^{\star}H_1^{\star}}{r+R^{\star}}\right)\frac{\partial H_1^{\star}}{\partial s}\right.\\&\quad\left.+H_2^{\star}\frac{\partial H_1^{\star}}{\partial r}+\frac{H_1^{\star}H_2^{\star}}{r+R^{\star}}\right),\end{aligned} \tag{4}$$

$$\begin{aligned}&\left(\frac{R^{\star}}{r+R^{\star}}\right)\left(U^{\star}\frac{\partial H_1^{\star}}{\partial s}\right)+\frac{H_1^{\star}H_2^{\star}}{r+R^{\star}}+V^{\star}\frac{\partial H_1^{\star}}{\partial r}\\&\quad-\left(\frac{R^{\star}H_1^{\star}}{r+R^{\star}}\frac{\partial U^{\star}}{\partial S}+\frac{V^{\star}U^{\star}}{r+R^{\star}}+H_2^{\star}\frac{\partial V^{\star}}{\partial r}\right)\\&\quad=\mu_e^{\star}\left(\frac{\partial^2 H_1^{\star}}{\partial r^2}-\frac{H_1^{\star}}{(r+R^{\star})^2}+\frac{1}{r+R^{\star}}\frac{\partial H_1^{\star}}{\partial r}\right),\end{aligned} \tag{5}$$

$$\begin{aligned}&V^{\star}\frac{\partial N^{\star}}{\partial r}+\frac{R^{\star}U^{\star}}{r+R^{\star}}\frac{\partial N^{\star}}{\partial s}\\&\quad=\frac{1}{\breve{\rho}_{nf}}\left(\breve{\mu}_{nf}+\frac{K_1^{\star}}{2}\right)\left(\frac{1}{r+R^{\star}}\frac{\partial N^{\star}}{\partial r}+\frac{\partial^2 N^{\star}}{\partial r^2}\right)\\&\quad\quad-\frac{K_1^{\star}}{2\breve{\rho}_{nf}}\left(\frac{\partial U^{\star}}{\partial r}+2N^{\star}+\frac{U^{\star}}{r+R^{\star}}\right),\end{aligned} \tag{6}$$

$$\frac{R^{\star}U^{\star}}{r+R^{\star}}\frac{\partial T^{\star}}{\partial s}+V^{\star}\frac{\partial T^{\star}}{\partial r}=\frac{\breve{k}_{nf}}{(\overline{\rho C_p})_{nf}}\left(\frac{1}{r+R^{\star}}\frac{\partial T^{\star}}{\partial r}+\frac{\partial^2 T^{\star}}{\partial r^2}\right), \tag{7}$$

The Eqs. (1)–(7) represent the nonlinear flow model of micropolar nanofluid over a curved Riga sheet. The physical quantities incorporated in these constitutive relations are thermal conductivity ($\breve{k}_{nf}$), heat capacitance ($(\overline{\rho C_p})_{nf}$), effective density ($\breve{\rho}_{nf}$), dynamic viscosity ($\breve{\mu}_{nf}$), and pressure ($p^{\star}$). Moreover, the conservation of mass, momentum, and the energy constitutive relations are described by Eqs. (1), (3–5), and (7).

The boundary conditions associated with the particular nanofluid flow model are described below:

$$\left.\begin{aligned}&\text{At curved Riga surface } r\to 0\\&V^{\star}=0\\&U^{\star}=al\exp\left(\frac{s}{l}\right)+L\left(kN^{\star}+\frac{U^{\star}}{r+R^{\star}}+\frac{\partial U^{\star}}{\partial r}\right)\\&T^{\star}=T_w^{\star}+\frac{\lambda_1^{\star}\breve{k}_{nf}}{k_f}\frac{\partial T^{\star}}{\partial r}\\&\frac{\partial H_1^{\star}}{\partial r}=H_2^{\star}=0\\&N^{\star}=-n\frac{\partial U^{\star}}{\partial r}\\&\text{Away from the Riga surface } r\to\infty\\&U^{\star}\to 0\\&H_1^{\star}\to H_e(s)=H_0^{\star}l\exp\left(\frac{s}{l}\right)\\&T^{\star}\to T_{\infty}^{\star}\\&N^{\star}\to 0\end{aligned}\right\}, \tag{8}$$

2.3 Similarity transformations

The similarity variables that support the particular nanofluid model over curved Riga surface are as follows:

$$\left.\begin{aligned} T^\star &= T_w^\star + (T_\infty^\star - T_w^\star)\beta(\eta) \\ \eta &= \sqrt{\frac{a}{\nu_f}}\, r \\ U^\star &= la\, \exp\left(\frac{s}{l}\right) F'(\eta) \\ V^\star &= -\left(\frac{R^\star}{r+R^\star}\right)\frac{1}{l}\sqrt{a\nu_f}\, \exp\left(\frac{s}{l}\right) F(\eta) \\ N^\star &= \sqrt{a\nu_f}\, \exp\left(\frac{s}{l}\right) H(\eta) \\ P^\star &= \rho^\star l^2 \exp\left(\frac{2s}{l}\right) p(\eta) \\ H_1^\star &= H_0^\star l \exp\left(\frac{s}{l}\right) G'(\eta) \\ H_2^\star &= -H_0^\star \left(\frac{R^\star}{r+R^\star}\right)\sqrt{\frac{\nu_f}{a}}\, \exp\left(\frac{s}{l}\right) G(\eta) \end{aligned}\right\}, \tag{9}$$

2.4 Effective characteristics of nanofluids

To improve the effective characteristics of the nanofluids, the following effective nanofluid models are used [17]:

$$\breve{\rho}_{nf} = \left[(1-\phi) + \frac{\phi\breve{\rho}_{cnt}}{\breve{\rho}_f}\right]\breve{\rho}_f, \tag{10}$$

$$(\overline{\rho C_p})_{nf} = \left[(1-\phi) + \frac{\phi(\overline{\rho C_p})_{cnt}}{(\overline{\rho C_p})_f}\right](\overline{\rho C_p})_f, \tag{11}$$

$$\breve{\mu}_{nf} = \breve{\mu}_f (1-\phi)^{-2.5}, \tag{12}$$

$$\breve{k}_{nf} = \frac{\breve{k}_f\left(1 - \frac{\breve{k}_f}{\breve{k}_{cnt}}\frac{L}{R}\phi^{0.2} + \left(1 - \frac{\breve{k}_f}{\breve{k}_{cnt}}\right)\phi\frac{L}{R}\phi^{0.2} + 2\phi\frac{\breve{k}_{cnt}}{\breve{k}_{cnt}-\breve{k}_f}\ln\left(\frac{\breve{k}_{cnt}+\breve{k}_f}{2\breve{k}_f}\right)\right)}{1-\phi+2\phi\left(\frac{\breve{k}_{cnt}}{\breve{k}_{cnt}-\breve{k}_f}\right)\ln\left(\frac{\breve{k}_{cnt}+\breve{k}_f}{2\breve{k}_f}\right)}, \tag{13}$$

$$\breve{k}_{nf} = \frac{\breve{k}_f\left(1-\phi-2\phi\left(\frac{\breve{k}_{cnt}}{\breve{k}_{cnt}-\breve{k}_f}\right)\ln\left(\frac{\breve{k}_{cnt}+\breve{k}_f}{2\breve{k}_f}\right)\right)}{1-\phi+2\phi\left(\frac{\breve{k}_{cnt}}{\breve{k}_{cnt}-\breve{k}_f}\right)\ln\left(\frac{\breve{k}_{cnt}+\breve{k}_f}{2\breve{k}_f}\right)}. \tag{14}$$

The effective density, heat capacity, volume fraction, dynamic viscosity, and thermal conductivity of the nanofluid are denoted by $\breve{\rho}_{nf}$, $(\overline{\rho C_p})_{nf}$, ϕ, $\breve{\mu}_{nf}$, and $\breve{k}_{nf}$, respectively.

2.5 First nanofluid model

By implementing the invertible variables, appropriate differentiation, effective nanofluid models, and Yamada and Ota thermal conductivity model described in Eq. (13), the following nanofluid model is obtained:

$$\begin{aligned} &\frac{1}{\left((1-\phi)+\frac{\phi\breve{\rho}_{cnt}}{\breve{\rho}_f}\right)}\left(\frac{1}{1-\phi^{2.5}}+K_1^\star\right)\left(F'''' + \frac{2F'''}{(k+\eta)} + \frac{F'}{(k+\eta)^3} - \frac{F''}{(k+\eta)^2}\right) \\ &+ \frac{R_1 k}{(k+\eta)}(FF'' - F''F') + \frac{R_1}{(k+\eta)^2}(FF'' - F'^2) \\ &- \frac{R_1 k}{(k+\eta)^3}FF' - \frac{1}{\left((1-\phi)+\frac{\phi\breve{\rho}_{cnt}}{\breve{\rho}_f}\right)}R_1 K_1^\star H' \\ &- \omega^\star\Theta\exp(-\omega^\star\eta) + \frac{\beta^\star}{(k+\eta)}\left(G'G'' + \frac{GG'}{(k+\eta)^2} - GG'' - \frac{G'G' + GG''}{(k+\eta)}\right) = 0, \end{aligned} \tag{15}$$

$$\begin{aligned} &\lambda^\star\left(G''' + \frac{G''}{(k+\eta)} - \frac{G'}{(k+\eta)^2}\right) \\ &+ R_1\left(\frac{k}{(k+\eta)}G'F' - \frac{k^2}{(k+\eta)^3}GF + \frac{k^2}{(k+\eta)^2}GF' - \frac{k}{(k+\eta)^2}FF'\right. \\ &\left. - R_1\left(\frac{k}{(k+\eta)}G'F' - \frac{k}{(k+\eta)^2}GG' - \frac{k}{(k+\eta)}FG''\right)\right) = 0, \end{aligned} \tag{16}$$

$$\begin{aligned} &\frac{1}{\left((1-\phi)+\frac{\phi\breve{\rho}_{cnt}}{\breve{\rho}_f}\right)}\left(\frac{1}{1-\phi^{2.5}}+\frac{K_1^\star}{2}\right)\left(H'' + \frac{H'}{(k+\eta)}\right) \\ &- \frac{R_1}{2}\frac{K_1^\star}{(k+\eta)}F'H + \frac{R_1}{2}\frac{K_1^\star}{(k+\eta)}H'F \\ &- \frac{1}{\left((1-\phi)+\frac{\phi\breve{\rho}_{cnt}}{\breve{\rho}_f}\right)}\frac{R_1 K_1^\star}{2}\left(2H + F'' + \frac{F'}{(k+\eta)}\right) = 0, \end{aligned} \tag{17}$$

$$\begin{aligned} &\frac{\frac{\breve{k}_f\left(1-\frac{\breve{k}_f}{\breve{k}_{cnt}}\frac{L}{R}\phi^{0.2}+\left(1-\frac{\breve{k}_f}{\breve{k}_{cnt}}\right)\phi\frac{L}{R}\phi^{0.2}+2\phi\frac{\breve{k}_{cnt}}{\breve{k}_{cnt}-\breve{k}_f}\ln\left(\frac{\breve{k}_{cnt}+\breve{k}_f}{2\breve{k}_f}\right)\right)}{1-\phi+2\phi\left(\frac{\breve{k}_{cnt}}{\breve{k}_{cnt}-\breve{k}_f}\right)\ln\left(\frac{\breve{k}_{cnt}+\breve{k}_f}{2\breve{k}_f}\right)}}{(1-\phi)+\frac{\phi(\overline{\rho C_p})_{cnt}}{(\overline{\rho C_p})_f}} \\ &\left(\beta'' + \frac{1}{(k+\eta)}\beta'\right) + \frac{kR_1}{(k+\eta)}\beta' F - \frac{kR_1}{(k+\eta)}\beta = 0. \end{aligned} \tag{18}$$

The supporting boundary conditions for the first model are defined as:

$$\left.\begin{aligned}
&\text{At the curved Riga surface } \eta = 0\\
&F'(\eta) = 1 + \gamma\left(\frac{1}{k}F'(\eta) + F''(\eta)(1-n)\right)\\
&F(\eta) = S\\
&H(\eta) = F''(\eta)n\\
&G(\eta) = 0\\
&G''(\eta) = 0\\
&\beta(\eta)\\
&\quad = 1 + M\frac{\breve{k}_f\left(1 - \frac{\breve{k}_f}{\breve{k}_{cnt}}\frac{L}{R}\phi^{0.2} + \left(1 - \frac{\breve{k}_f}{\breve{k}_{cnt}}\right)\phi\frac{L}{R}\phi^{0.2} + 2\phi\frac{\breve{k}_{cnt}}{\breve{k}_{cnt}-\breve{k}_f}\ln\left(\frac{\breve{k}_{cnt}+\breve{k}_f}{2\breve{k}_f}\right)\right)}{1-\phi+2\phi\left(\frac{\breve{k}_{cnt}}{\breve{k}_{cnt}-\breve{k}_f}\right)\ln\left(\frac{\breve{k}_{cnt}+\breve{k}_f}{2\breve{k}_f}\right)}\beta(\eta)\\
&\text{Far from the Riga surface } \eta \to \infty\\
&F'(\eta) = 0\\
&F''(\eta) = 0\\
&H(\eta) = 0\\
&G'(\eta) = 1\\
&\beta(\eta) = 0
\end{aligned}\right\}, \tag{19}$$

2.6 Second nanofluid model

By implementing the second thermal conductivity model described in Eq. (14) which is known as Xue model, the following dimensionless nanofluid model is obtained after the successful calculation:

$$\begin{aligned}
&\frac{1}{\left((1-\phi)+\frac{\phi\breve{\rho}_{cnt}}{\breve{\rho}_f}\right)}\left(\frac{1}{1-\phi^{2.5}}+K_1^\star\right)\left(F''''+\frac{2F''''}{(k+\eta)}+\frac{F'}{(k+\eta)^3}\right.\\
&\quad\left.-\frac{F''}{(k+\eta)^2}\right)+\frac{R_1k}{(k+\eta)}(FF''-F''F')\\
&\quad+\frac{R_1}{(k+\eta)^2}(FF''-F'^2)-\frac{R_1k}{(k+\eta)^3}FF'\\
&\quad-\frac{1}{\left((1-\phi)+\frac{\phi\breve{\rho}_{cnt}}{\breve{\rho}_f}\right)}R_1K_1^\star H'-\omega^\star\Theta\exp(-\omega^\star\eta)\\
&+\frac{\beta^\star}{(k+\eta)}\left(G'G''+\frac{GG'}{(k+\eta)^2}-GG''-\frac{G'G'+GG''}{(k+\eta)}\right)=0,
\end{aligned} \tag{20}$$

$$\begin{aligned}
&\lambda^\star\left(G''''+\frac{G''}{(k+\eta)}-\frac{G'}{(k+\eta)^2}\right)\\
&\quad+R_1\left(\frac{k}{(k+\eta)}G'F'-\frac{k^2}{(k+\eta)^3}GF+\frac{k^2}{(k+\eta)^2}GF'\right.\\
&\quad-\frac{k}{(k+\eta)^2}FF'-R_1\left(\frac{k}{(k+\eta)}G'F'-\frac{k}{(k+\eta)^2}GG'\right.\\
&\quad\left.\left.-\frac{k}{(k+\eta)}FG''\right)\right)=0,
\end{aligned} \tag{21}$$

$$\begin{aligned}
&\frac{1}{\left((1-\phi)+\frac{\phi\breve{\rho}_{cnt}}{\breve{\rho}_f}\right)}\left(\frac{1}{1-\phi^{2.5}}+\frac{K_1^\star}{2}\right)\left(H''+\frac{H'}{(k+\eta)}\right)\\
&\quad-\frac{R_1}{2}\frac{K_1^\star}{(k+\eta)}F'H+\frac{R_1}{2}\frac{K_1^\star}{(k+\eta)}H'F\\
&\quad-\frac{1}{\left((1-\phi)+\frac{\phi\breve{\rho}_{cnt}}{\breve{\rho}_f}\right)}\frac{R_1K_1^\star}{2}\left(2H+F''+\frac{F'}{(k+\eta)}\right)=0,
\end{aligned} \tag{22}$$

$$\begin{aligned}
&\frac{\frac{\breve{k}_f\left(1-\phi-2\phi\left(\frac{\breve{k}_{cnt}}{\breve{k}_{cnt}-\breve{k}_f}\right)ln\left(\frac{\breve{k}_{cnt}+\breve{k}_f}{2\breve{k}_f}\right)\right)}{1-\phi+2\phi\left(\frac{\breve{k}_{cnt}}{\breve{k}_{cnt}-\breve{k}_f}\right)\ln\left(\frac{\breve{k}_{cnt}+\breve{k}_f}{2\breve{k}_f}\right)}}{(1-\phi)+\frac{\phi(\overline{\rho C_p})_{cnt}}{(\overline{\rho C_p})_f}}\left(\beta''+\frac{1}{(k+\eta)}\beta'\right)\\
&\quad+\frac{kR_1}{(k+\eta)}\beta'F-\frac{kR_1}{(k+\eta)}\beta=0,
\end{aligned} \tag{23}$$

The supporting boundary conditions for the second nanofluid model are as under:

$$\left.\begin{aligned}
&\text{At the curved Riga surface } \eta = 0\\
&F'(\eta) = 1 + \gamma\left(\frac{1}{k}F'(\eta) + F''(\eta)(1-n)\right)\\
&F(\eta) = S\\
&H(\eta) = F''(\eta)n\\
&G(\eta) = 0\\
&G''(\eta) = 0\\
&\beta(\eta) = 1 + M\frac{\breve{\breve{k}}_f\left(1-\phi-2\phi\left(\frac{\breve{k}_{cnt}}{\breve{k}_{cnt}-\breve{k}_f}\right)\ln\left(\frac{\breve{k}_{cnt}+\breve{k}_f}{2\breve{k}_f}\right)\right)}{1-\phi+2\phi\left(\frac{\breve{k}_{cnt}}{\breve{k}_{cnt}-\breve{k}_f}\right)\ln\left(\frac{\breve{k}_{cnt}+\breve{k}_f}{2\breve{k}_f}\right)}\beta(\eta)\\
&\text{Far from the Riga surface } \eta \to \infty\\
&F'(\eta) = 0\\
&F''(\eta) = 0\\
&H(\eta) = 0\\
&G'(\eta) = 1\\
&\beta(\eta) = 0
\end{aligned}\right\}. \tag{24}$$

2.7 Quantities of engineering interest

The local thermal transport and wall shear stresses are very important from engineering aspects. The formulas for these quantities are as under:

$$C_F = \frac{\tau_{rs}}{\breve{\breve{\rho}}_{nf}u_w^2}, \tag{25}$$

$$\mathrm{Nu} = \frac{q_w s}{\breve{\breve{k}}_{nf}(T_w^\star - T_\infty^\star)}, \tag{26}$$

The shear stresses and heat flux are given in the following formulas:

$$\tau_{rs} = \frac{1}{\breve{\rho}_{nf}}(\breve{\mu}_{nf} + K_1^{\star})\left(\frac{\partial U^{\star}}{\partial r} + \frac{U^{\star}}{r + R^{\star}} + kU^{\star}\right)\downarrow_{r=0}, \quad (27)$$

$$q_w = -\breve{\breve{k}}_{nf}\left(\frac{\partial T^{\star}}{\partial r}\right), \quad (28)$$

By using the formulas described in Eqs. (27) and (28) in Eqs. (25) and (26), the following skin friction and Nusselt number expressions are obtained:

$$\mathrm{Re}_s^{1/2} = \frac{1}{(1-\phi) + \frac{\phi\breve{\rho}_{cnt}}{\breve{\rho}_f}}\left(\frac{1}{1-\phi^{2.5}} + K_1^{\star}\right) \times \left(F''(\eta) + \frac{F'(\eta)}{k} - nK_1^{\star}F''(\eta)\right)\downarrow_{\eta=0}, \quad (29)$$

Nusselt number expression for the first nanofluid model

$$\sqrt{\mathrm{Re}_s}\,\mathrm{Nu}_s = -\frac{\breve{k}_f\left(1 - \frac{\breve{k}_f}{\breve{k}_{\mathrm{cnt}}}\frac{L}{R}\phi^{0.2} + \left(1 - \frac{\breve{k}_f}{\breve{k}_{\mathrm{cnt}}}\right)\phi\frac{L}{R}\phi^{0.2} + 2\phi\frac{\breve{k}_{\mathrm{cnt}}}{\breve{k}_{\mathrm{cnt}} - \breve{k}_f}\ln\left(\frac{\breve{k}_{\mathrm{cnt}} + \breve{k}_f}{2\breve{k}_f}\right)\right)}{1 - \phi + 2\phi\left(\frac{\breve{k}_{\mathrm{cnt}}}{\breve{k}_{\mathrm{cnt}}\breve{k}_f}\right)\ln\left(\frac{\breve{k}_{\mathrm{cnt}} + \breve{k}_f}{2\breve{k}_f}\right)}\beta'(0)$$

Nusselt number expression for the second nanofluid model

$$\sqrt{\mathrm{Re}_s}\,\mathrm{Nu}_s = -\frac{\breve{k}_f\left(1 - \phi - 2\phi\left(\frac{\breve{k}_{\mathrm{cnt}}}{\breve{k}_{\mathrm{cnt}} - \breve{k}_f}\right)\ln\left(\frac{\breve{k}_{\mathrm{cnt}} + \breve{k}_f}{2\breve{k}_f}\right)\right)}{1 - \phi + 2\phi\left(\frac{\breve{k}_{\mathrm{cnt}}}{\breve{k}_{\mathrm{cnt}} - \breve{k}_f}\right)\ln\left(\frac{\breve{k}_{\mathrm{cnt}} + \breve{k}_f}{2\breve{k}_f}\right)}\beta'(0) \quad (30)$$

where $\mathrm{Re}_s = \left(\frac{au_w}{\nu_f}\right)$.

3 Mathematical analysis

The above described two nanofluid models are highly nonlinear coupled and tedious systems. For such nature

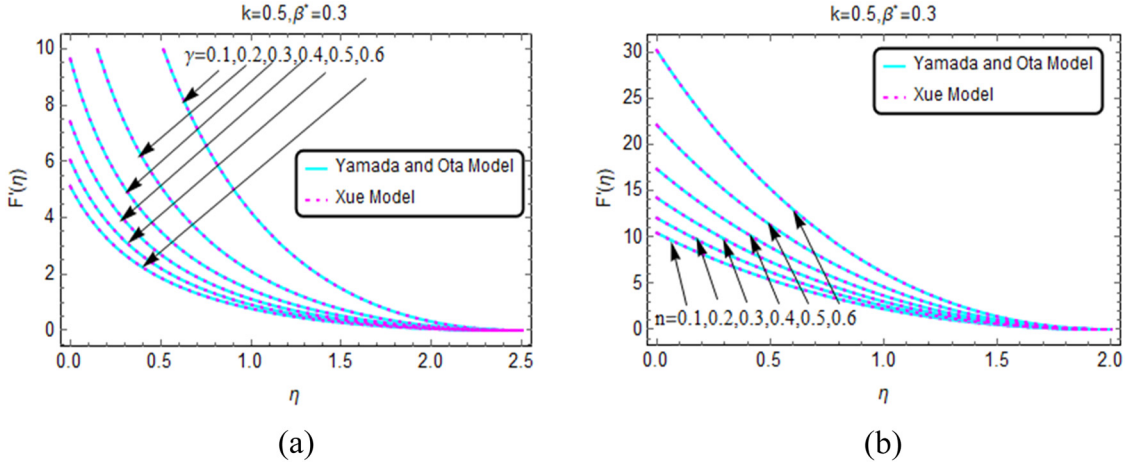

Figure 2: $F'(\eta)$ against (a) γ and (b) n.

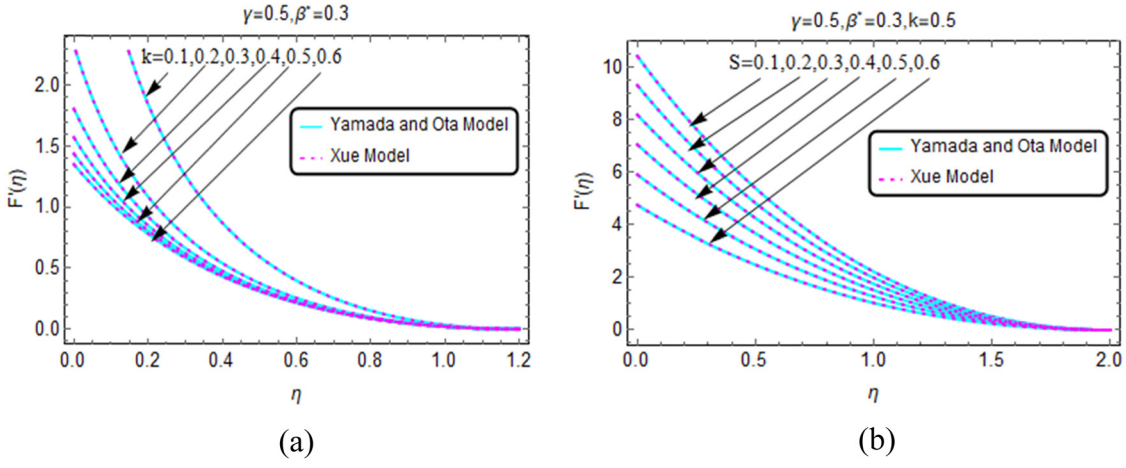

Figure 3: $F'(\eta)$ against (a) k and (b) S.

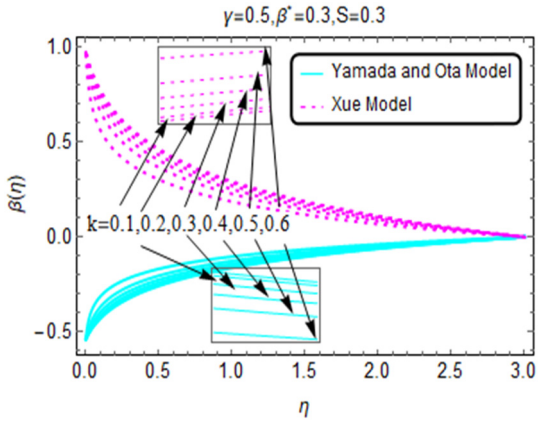

Figure 4: $\beta(\eta)$ for varying k.

of nanofluid models, analytical solutions are not reliable. Therefore, numerical approach is the best option to tackle such nanofluid models. Thus, numerical technique known as RK method together with Shooting technique [18] is implemented to tackle the particular nanofluid models.

To initiate the said technique, the higher order system needs to reduce into first order initial value problem. Thus, the following transformations are made that transformed the particular models into a desired system:

$$\left.\begin{aligned} &b_1^\star = F,\ b_2^\star = F',\ b_3^\star = F'',\ b_4^\star = F''',\\ &b_5^\star = G,\ b_6^\star = G',\ b_7^\star = G'',\\ &b_8^\star = H,\ b_9^\star = H',\\ &b_{10}^\star = \beta,\ b_{11}^\star = \beta', \end{aligned}\right\}, \tag{31}$$

As the models are lengthy, we only defined the transformations and incorporated the results for the flow regimes. For further computations, MATHEMATICA 10.0 is used.

4 Results and discussion

This subsection organized is to examine the nanofluid flow behavior against Yamada and Ota and Xue models.

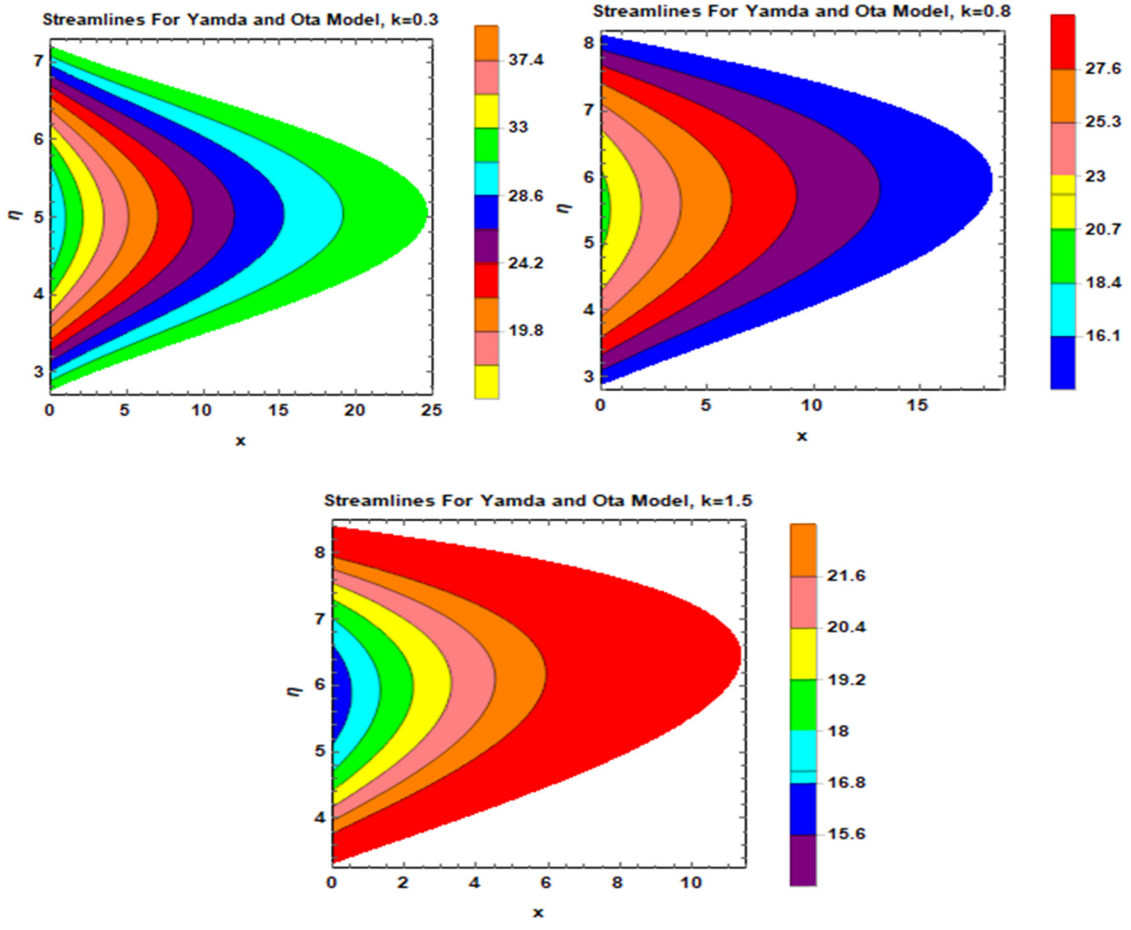

Figure 5: Streamlines for varying curvature.

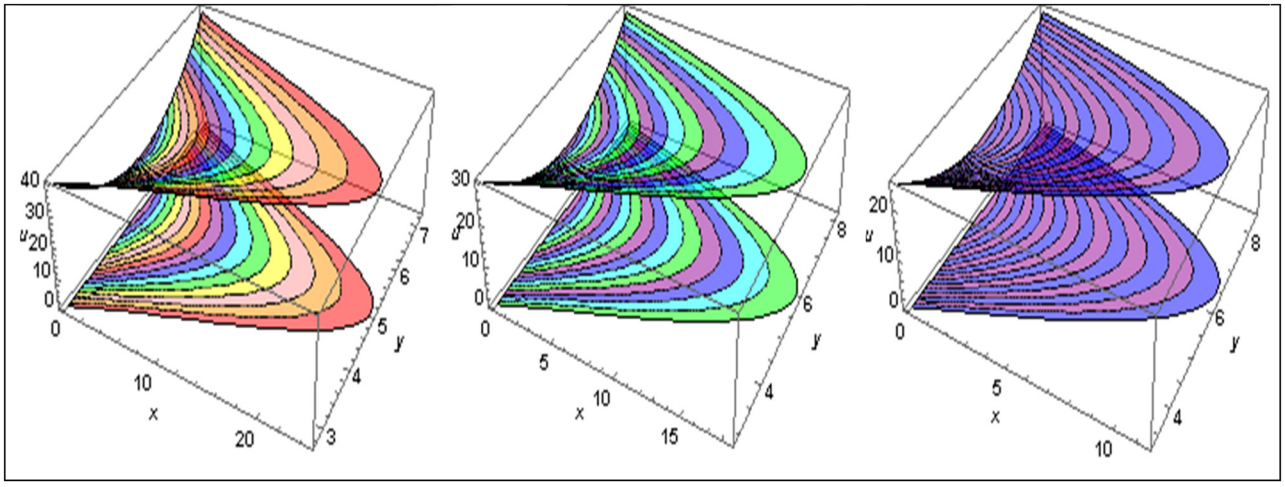

Figure 6: 3D view of streamlines for varying curvature.

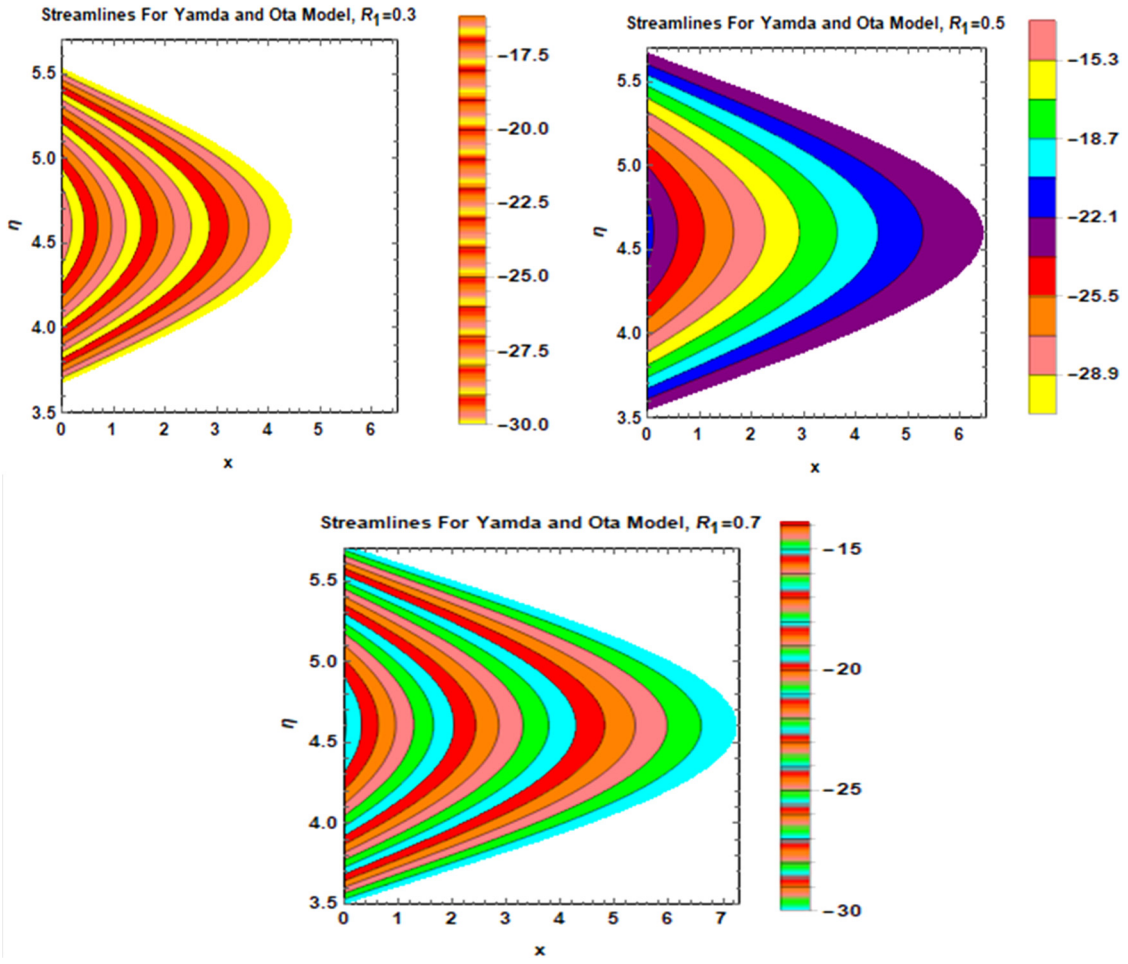

Figure 7: Streamlines for varying R_1.

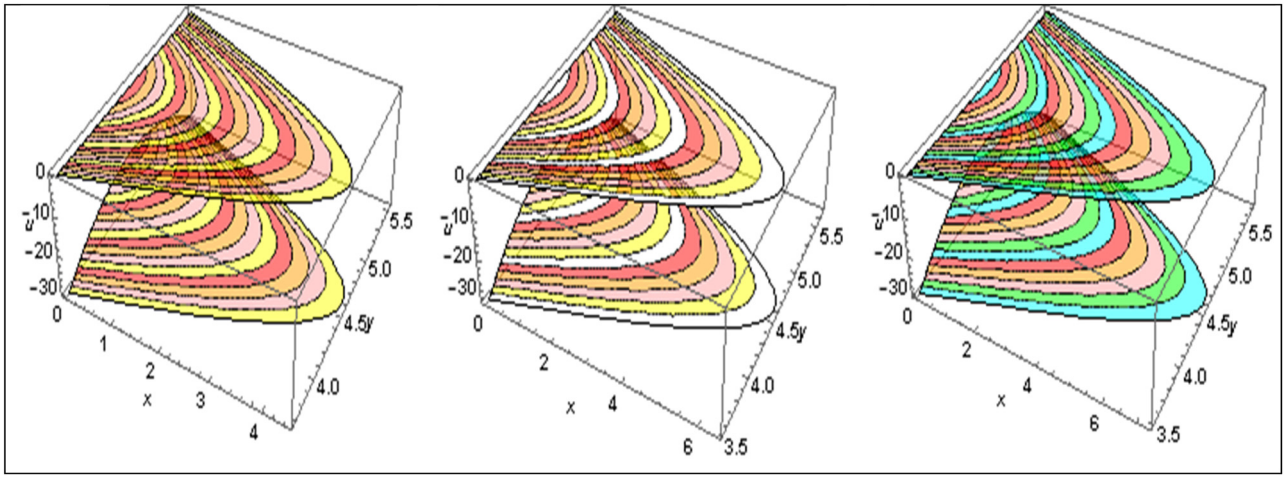

Figure 8: 3D view of streamlines for varying R_1.

The velocity and temperature trends are decorated with various pre-eminent flow parameters.

The velocity $F'(\eta)$ against the partial slip parameter γ are painted in Figure 2a. By inspection of the results, it is perceived that the velocity of SWCNTs-H_2O declines for higher thermal slip effects. Physically, the effects of frictional force are stronger near the surface and the fluid particles adjacent to it. Due to high frictional effects, the

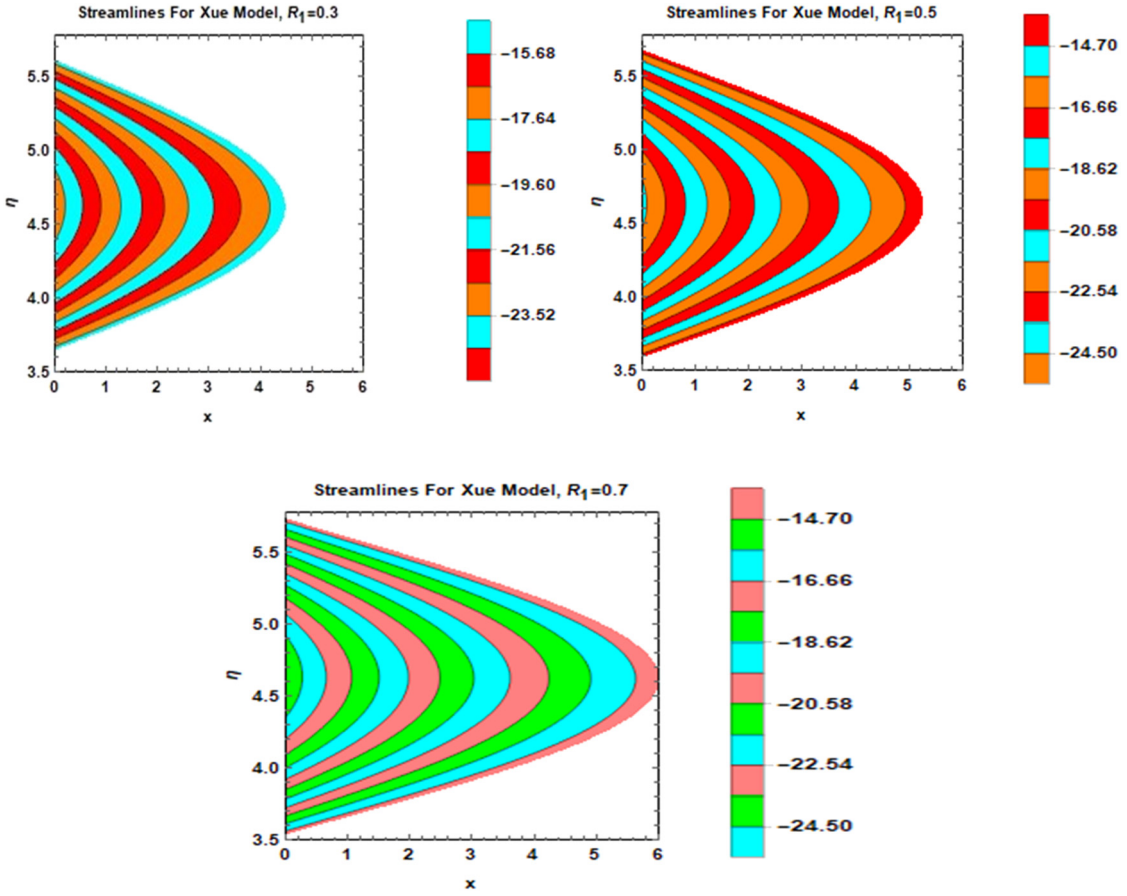

Figure 9: Streamlines' behavior for R_1 for Xue model.

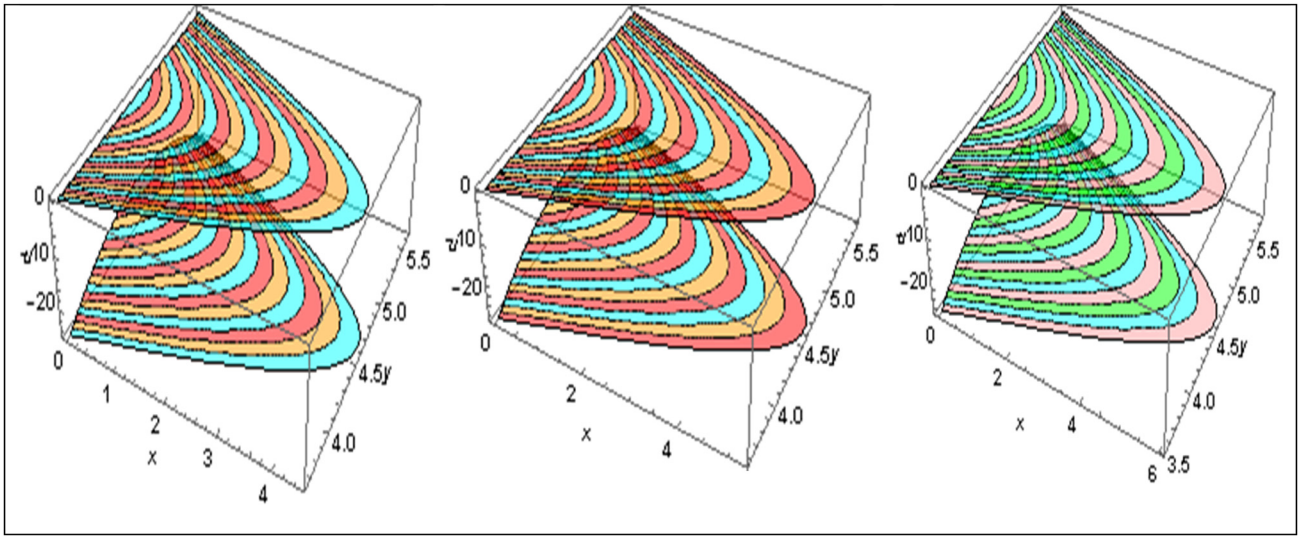

Figure 10: 3D view of streamlines for R_1 for Xue model.

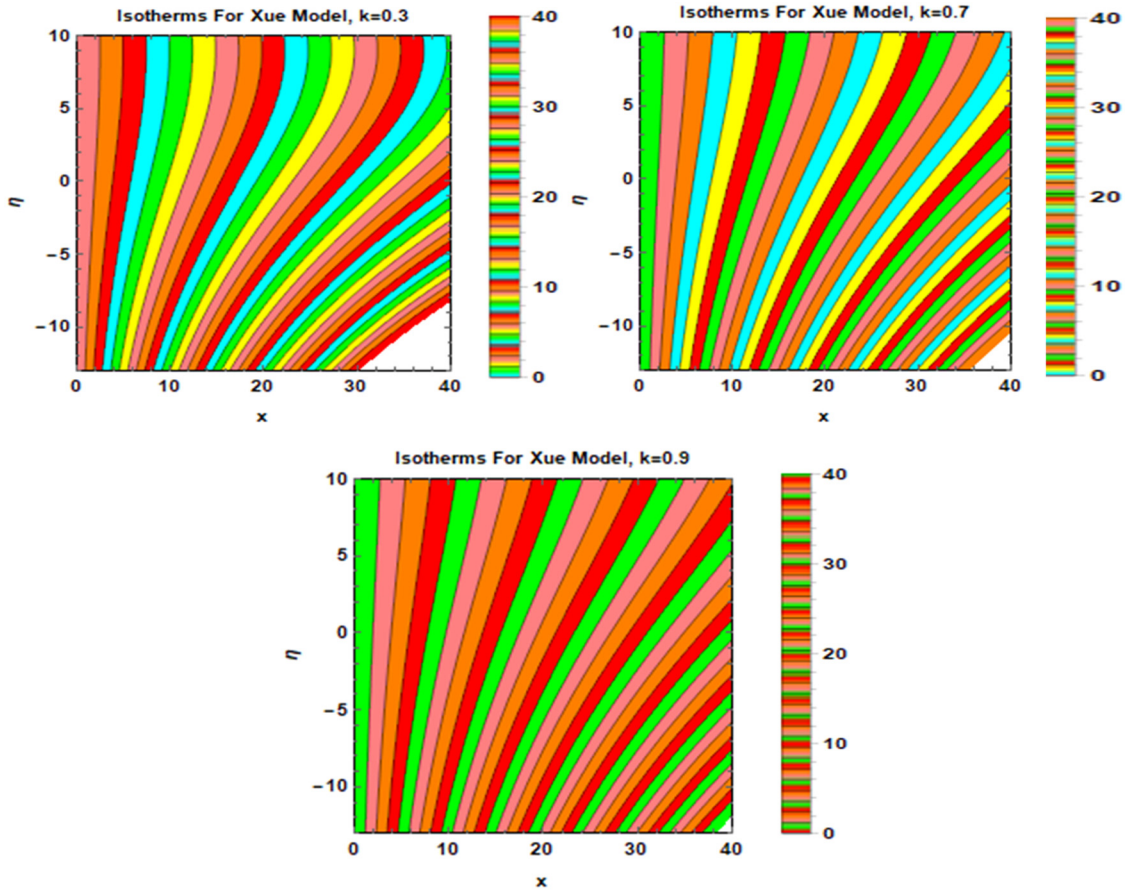

Figure 11: Isotherms profile for varying curvature.

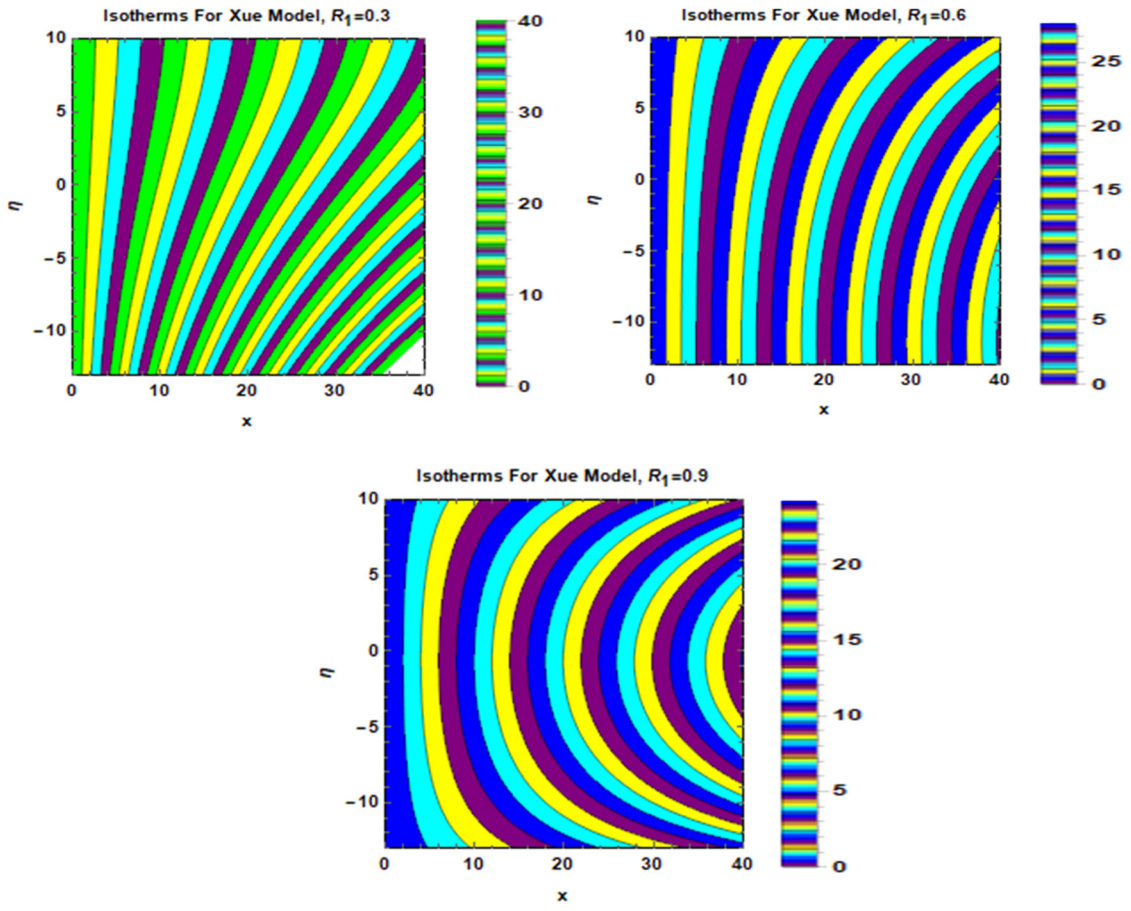

Figure 12: Isotherms profile for varying R_1.

velocity drops promptly in this region. Apart from the surface, the velocity decrement becomes slow because the frictional force becomes weaker between the fluid layers. The velocity against microgyration number n is decorated in Figure 2b. It is pointed that due to microgyration effects, the velocity of the nanofluid enhances. Physically, due to the saturation of microgyration in the nanofluid, the frictional effects near the surface and the fluid layer adjacent to it reduced. Therefore, the velocity starts increasing abruptly in this region. Far from the surface, increasing trends in the nanofluid velocity becomes almost inconsequential.

The curvature effects on the velocity trends of SWCNTs-H_2O are elucidated in Figure 3a. From the plotted results, it is examined that the velocity of SWCNTs-H_2O drops for larger curvature of the surface. Physically, the surface becomes more bent against the larger curvature which resists the fluid particles; consequently, motion of the fluid particles drops which leads to a decline in the velocity. Near the surface, maximum decrement is found due to high curvature effects and these effects becomes minimal far from the surface. Similarly, decreasing trends in $F'(\eta)$ are perceived in Figure 3b against increasing values of S.

The trends in thermal performance $\beta(\eta)$ against multiple values of surface curvature are decorated in Figure 4. From Figure 4, reverse trends in the temperature of the nanofluids are pointed while the curvature parameter varies. For Xue based thermal conductance nanofluid model, the temperature rises near the surface against variation in k. Physically, as the curvature for smaller curvature the fluid particles flow freely due to which the collision between the molecules rises which lead to abrupt changes in the temperature. On the other side, the temperature drops for Yamada and Ota based on thermal conductance correlation. For larger curved surface, maximum decrement is observed.

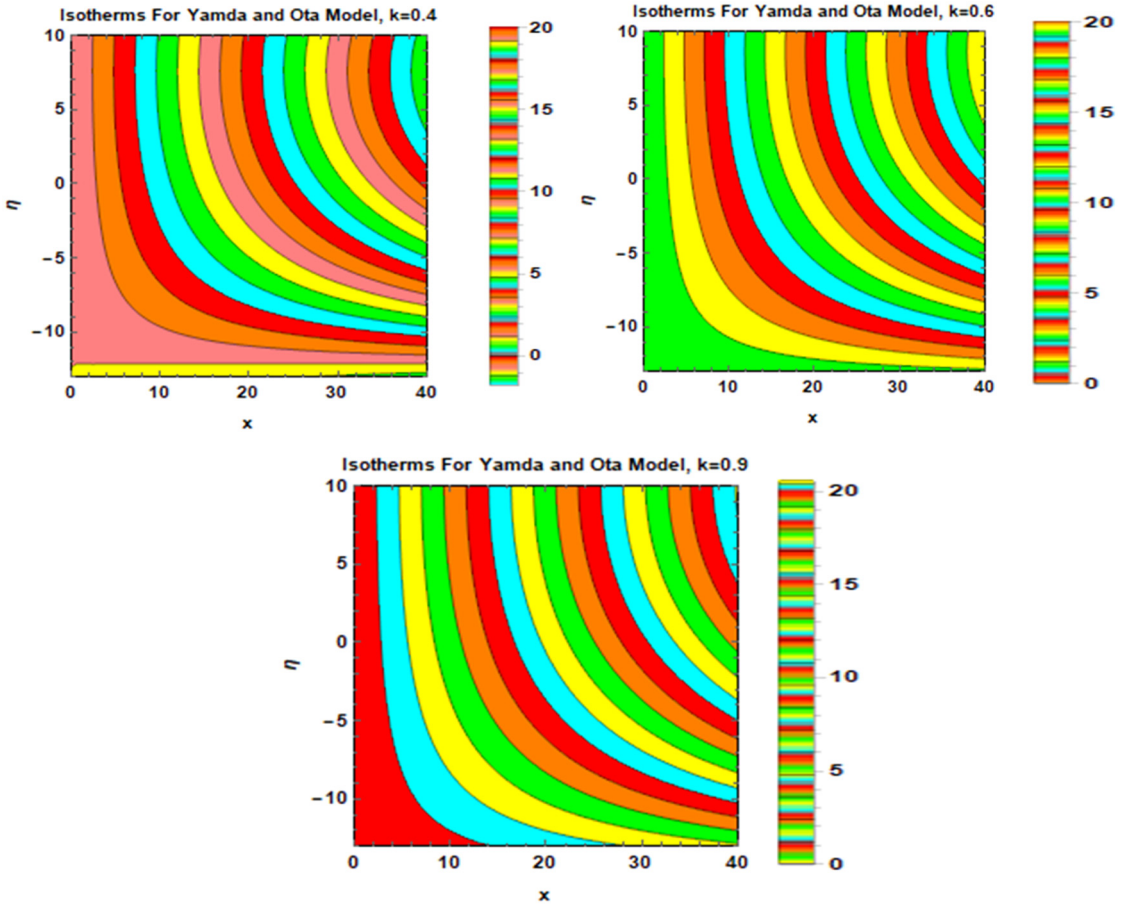

Figure 13: Isotherms profile for varying k and Yamada model.

4.1 Streamlines profile

The impact of multiple parameters on the streamline's behavior are decorated in Figures 5–10. 3D view of the streamlines against the preemenant flow parameters is also painted. The streamline's behavior for multiple surface curvature is painted in Figure 5, while corresponding 3D scenario is decorated in Figure 6. Deep penetration effects on the streamline's behavior are examined against smaller surface curvature and these are pointed in Figure 5. When the curvature rises, the streamlines bend vertically and the penetrating effects are reduced. At the mid portion of the surface, the streamline's shape is almost parabolic type, while against higher curvature the parabola bends vertically. Similarly, the trends in streamlines are elaborated by altering R_1 as shown in Figure 7. High penetrating effects are perceived for increase in R_1 and the parabolic streamlines shrinked towards the center of the surface. 3D view of the streamline's pattern for multiple R_1 is depicted in Figure 8. From Figure 9, fewer penetrating effects are detected against R_1 and 3D profile of the streamlines is displayed in Figure 10.

4.2 Isotherms profile

The trends of isotherms against the pre-eminent flow parameters are decorated in Figures 11–14. Figure 11 depicts the pattern of isotherms against surface curvature. More penetration in the isotherms is reflected against smaller curvature and it reduces for higher surface curvature. As the curvature increases, the isotherms become flat towards the horizontal axis. In Figure 12, the reverse pattern in isotherms is reflected for increase in R_1. More penetrating effects of isotherms are pointed for larger R_1. Figures 13 and 14 depict the behavior of isotherms for the surface curvature and R_1 against Yamada and Ota correlation based nanofluid. For this, more penetrating effects are reflected along vertical axis in both the cases.

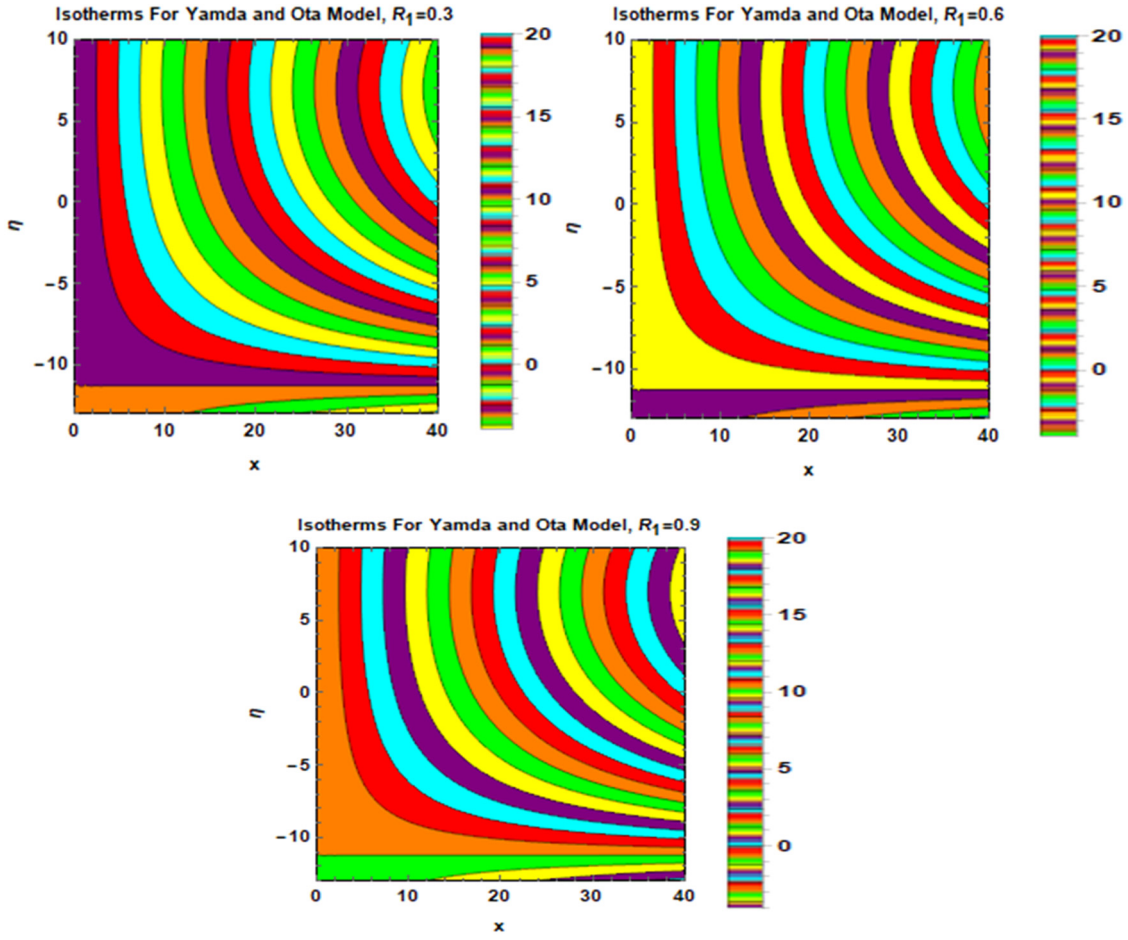

Figure 14: Isotherms profile for varying R_1 and Yamada model.

4.3 Thermophysical characteristics

The role of thermal conductivity is significant in the analysis of nanofluids. This subsection highlights the role of lengths, radius, and volumetric fraction of CNTs on thermal conductance. It is evident that with the increment in the length of CNTs, the thermal conductivity enhances abruptly. Also, it can be seen that larger radius of CNTs increases thermal conductivity of the nanofluid. The volumetric fraction is a significant parameter in the study of nanofluids. These effects on thermal conductivity are plotted and investigations show that for higher volume fraction, thermal conductivity increases abruptly (Figure 15).

4.4 Skin friction

The variations in shear stress for volume fraction, S, and curvature parameter are depicted in Figure 16. The volume fraction favors the shear stress and the direct relation between the volume fraction and shear stress is examined. Whereas the parameter S and increase in curvature oppose the shear stress. The inverse proportion relation between the parameter S and curvature of the Riga surface is investigated.

4.5 Authentication of the analysis

It is a prominent fact that the nanofluid models can be reduced into conventional fluid model as the volumetric fraction of the nanomaterial tends to zero. Therefore, a comparison is provided by imposing some restrictions on the nanofluid model. These are $S = 0$, $R_1 = 1$, $\beta^\star = 0$, $\Theta = 0$, $\gamma = 0$, $\phi = 0$, and $\omega = 0$, and the results are computed for $-\mathrm{Re}_s C_F$. From the numerical results, it is examined that the presented study is valid under aforementioned assumptions and is in excellent agreement with previous science literature (Table 1).

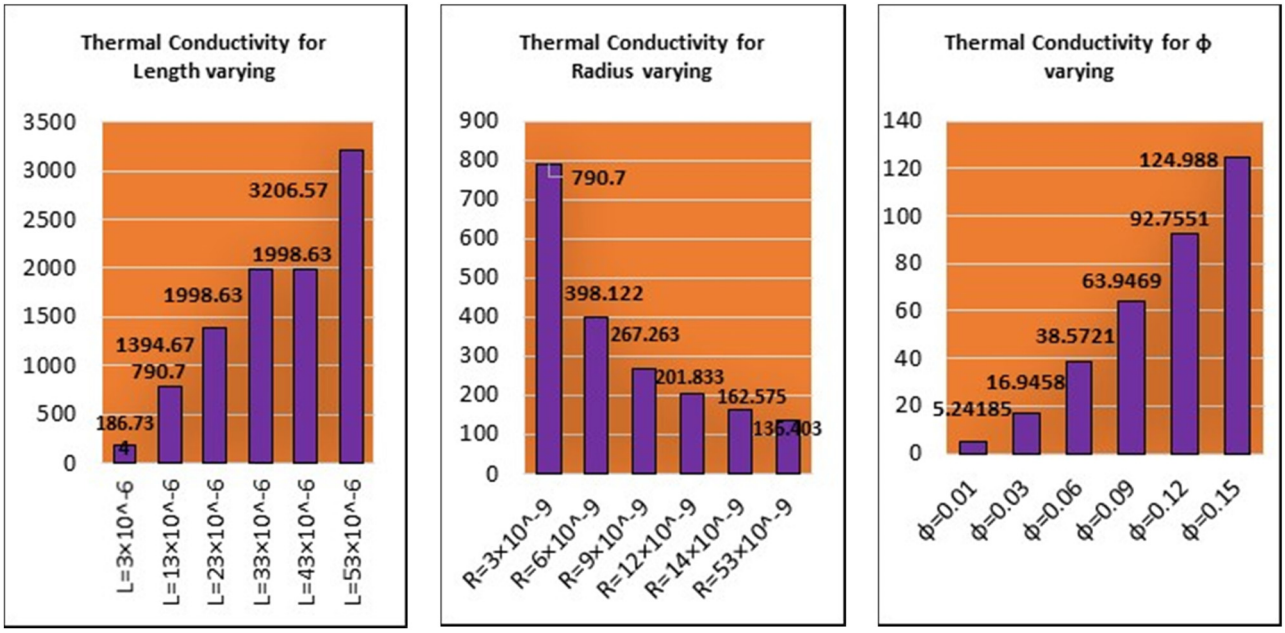

Figure 15: Effective characteristics of the nanofluids.

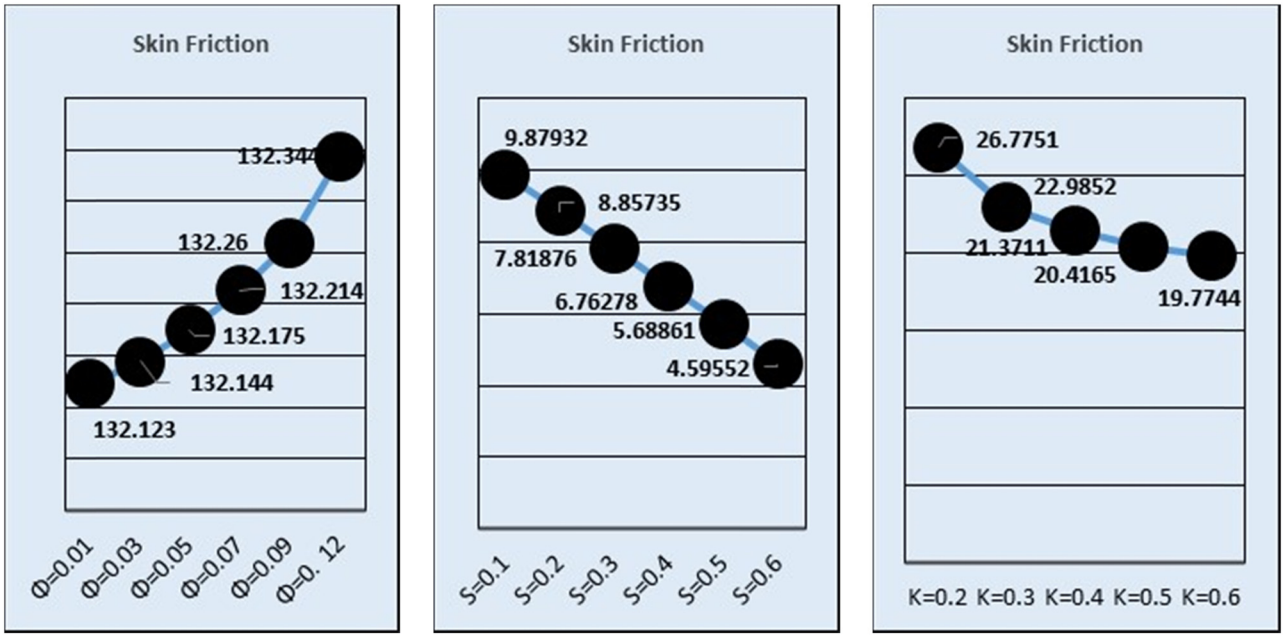

Figure 16: Skin friction for varying ϕ, S, and k.

Table 1: The validity of the analysis under certain parameter assumptions

k	Present	Sajid *et al.* [19]
5	0.757631	0.75763
10	0.873489	0.87349
20	0.93561	0.93561
30	0.970198	0.95686
40	0.942587	0.96759
50	0.974049	0.97405

5 Conclusion

The flow of SWCNTs-H_2O in the existence of velocity and thermal slip is conducted over a Riga geometry. For thermal enhancement, two different thermal conductance correlations are plugged in the energy equation. The resultant colloidal models were handled numerically. It is detected that the velocity promptly drops against higher surface curvature. The decrement in the nanofluid velocity is noticed for stronger partial slip parameter and it rises for microgyration parameter *n*. The thermal performance signifies for Xue based colloidal mixture and reverse variations are detected for Yamada and Ota based model. The local heat transfer rate enhances for both the models and prevailed trends are observed for Xue model. The high-volume fraction resists the shear stress.

Funding information: The author D. Baba Basha would like to thank the Deanship of Scientific research at Majmaah University for supporting this work under project number No. R-2022-57.

Author contributions: All authors have accepted responsibility for the entire content of this manuscript and approved its submission.

Conflict of interest: The authors state no conflict of interest.

References

[1] Bruggeman DAG. Berechnung verschiedener physikalischer konstanten von heterogenen substanzen,
I – Dielektrizitatskonstanten und leitfahigkeiten der mischkorper aus isotropen substanzen. Annalen der Physik Leipz. 1935;24:636–79.

[2] Hamilton HL, Crosser OK. Thermal conductivity of heterogeneous two-component systems. Ind Eng Chem Fundam. 1962;1(3):187–91.

[3] Koo J, Kleinstreuer C. Laminar nanofluid flow in micro-heat sinks. Int J Heat Mass Transf. 2005;48(13):2652–61.

[4] Koo J, Kleinstreuer C. A new thermal conductivity model for nanofluids. J Nanopart Res. 2004;6(6):577–88.

[5] Wasp FJ. Solid–liquid slurry pipeline transportation. Trans Techniques Berlin; 1977.

[6] Li CH, Peterson GP. Experimental investigation of temperature and volume fraction variations on the effective thermal conductivity of nanoparticle suspensions (nanofluids). J Appl Phys. 2006;99(8):084314.

[7] Patel HE, Sundararajan T, Das SK. An experimental investigation into the thermal conductivity enhancement in oxide and metallic nanofluids. J Nanopart Res. 2010;12:1015–31.

[8] Godson RL, Mohan LB, Wongwises DS. Experimental investigation on the thermal conductivity and viscosity of silver – deionized water nanofluid. Exp Heat Transf. 2010;23:317–32.

[9] Corcione M. Rayleigh–Bénard convection heat transfer in nanoparticle suspensions. Int J Heat Fluid Flow. 2011;32:65–77.

[10] Sheikholeslami M, Zia QMZ, Ellahi R. Influence of induced magnetic field on free convection of nanofluid considering Koo-Kleinstreuer-Li (KKL) correlation. Appl Sci. 2016;6(11):1–13.

[11] Xue QZ. Model for thermal conductivity of carbon nanotubes based composites. Nanotechnology. 2005;17:1655–60.

[12] Saleh SHM, Arifin NM, Nazar R, Pop I. Unsteady micropolar fluid over a permeable curved stretching shrinking surface. Math Probl Eng. 2017;2017:3085249. doi: 10.1155/2017/3085249.

[13] Ahmad L, Khan M. Numerical simulation for MHD flow of Sisko nanofluid over a moving curved surface: A revised model. Microsyst Technol. 2018;25:2411–28. doi: 10.1007/s00542-018-4128-3.

[14] Reddy JVR, Sugunamma V, Sandeep N. Dual solutions for nanofluid flow past a curved surface with nonlinear radiation, Soret and Dufour effects. J Phys. 2018;1000:012152. doi: 10.1088/1742-6596/1000/1/012152.

[15] Saba F, Ahmed N, Hussain S, Khan U, Mohyud-Din ST, Darus M. Thermal analysis of nanofluid flow over a curved stretching surface suspended by carbon nanotubes with internal heat generation. Appl Sci. 2018;8:1–15.

[16] Abbas N, Malik YM, Nadeem S. Transportation of magnetized micropolar hybrid nanomaterial fluid flow over a Riga curface surface. Comput Methods Programs Biomed. 2019;185:105136. doi: 10.1016/j.cmpb.2019.105136.

[17] Nadeem S, Khan AU, Hussain ST. Model based study of SWCNT and MWCNT thermal conductivities effect on the heat transfer due to the oscillating wall conditions. Int J Hydrog Energy. 2017;42:28945–57.

[18] Ahmed N, Khan AU, Mohyud-Din ST. Unsteady radiative flow of chemically reacting fluid over a convectively heated stretchable surface with cross-diffusion gradients. Int J Therm Sci. 2017;121:182–91.

[19] Sajid M, Ali N, Javed T, Abbas Z. Stretching a curved surface in a viscous fluid. Chin Phys Lett. 2010;27:024703. doi: 10.1088/0256-307X/27/2/024703.